JOURNAL OF MATERIALS SCIENCE 9 (1974) 229–239

The temperature-dependence of the mechanical properties of unidirectionally solidified silver-germanium eutectic

W. R. KRUMMHEUER*, H. ALEXANDER
Abteilung für Metallphysik im II. Physikalischen, Institut der Universität Köln, W. Germany

Work-hardening curves of the unidirectionally solidified silver-germanium eutectic have been determined by tensile deformation between room temperature and 615° C. The transition stress, σ_0 between elastic and plastic deformation of the germanium platelets, exhibits the same temperature dependence ($\sigma_0 \sim \exp Q/KT$) over the whole temperature range. σ_0 is determined, however, by two effects: the temperature-dependent critical shear stress of germanium and the lowering of the shear strength, τ, of the phase interfaces. Estimates of τ yield 14 kg mm^{-2} at room temperature and < 0.12 kg mm^{-2} at 615° C. At low temperatures (< 400° C), the composite fracture is initiated by the fracture of "fibres" (platelets), whereas at higher temperatures, the matrix fails first. As long as the interface shear strength is sufficiently large, the composite fracture is retarded resulting in a pronounced maximum of the fracture strain at 550° C.

1. Introduction

If a eutectic alloy of a fcc metal and an elemental semiconductor is produced by unidirectional solidification, a material with a filamentary or platelike microstructure can result [1-5]. These alloys consist of a fcc solid solution and a nearly pure semiconductor phase [6] and possess mechanical properties similar to those of fibre reinforced materials [4, 5]. As the ductility of a semiconductor is strongly temperature dependent [7], it is possible, merely by altering the temperature of deformation, to investigate the effect of both brittle and highly ductile fibres on the mechanical properties of such alloys. A complication arises, however, since the shear strength of the interface decreases with increasing temperature [5] and, hence, the effect of temperature on both ductility and interface shear strength must be considered when interpreting these mechanical properties.

In this work, a Ag-Ge eutectic was investigated, since the germanium brittle-ductile transition temperature is smaller than the eutectic temperature (651° C); the mechanical properties in compression and tension were investigated over a range of temperature.

2. Experimental

A eutectic Ag-Ge alloy with a nominal germanium content of 25.9 at. % [6] was produced from Degussa silver (99.995%) and zone refined germanium (specific resistivity > 45 Ω cm) by means of induction heating under vacuum ($p < 10^{-4}$ Torr).

Owing to the brittleness of this alloy at room temperature, the deformation specimens were prepared in final form by remelting and casting the alloy in a graphite mould. This mould (Fig. 1), which consisted of two identical halves held together by thin Mo wire, permitted two similar specimens to be prepared with shoulders sufficiently large to prevent failure at this point during subsequent deformation. The molten alloy was solidified in a steep temperature gradient (~ 200° C cm^{-1}) with a rate of solidification of 2 mm h^{-1} under vacuum ($p < 10^{-4}$ Torr) in order to produce the required microstructure.

After solidification, the specimens were separated with a jeweller's saw and the surface cleaned by etching (16 parts HNO_3 −60%, 5 parts HF −40%, 16 parts H_2O). Any surface roughening remaining was removed by careful

*Present address: Institut Technische Garne, ENKA GLANZSTOFF AG, Wuppertal.

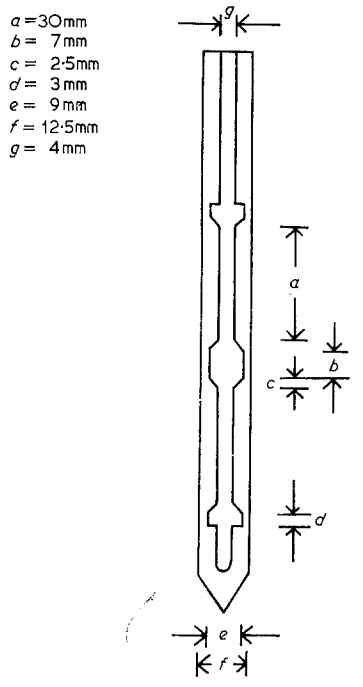

Figure 1 Form of the slot in each half of the crucible.

mechanical polishing and subsequent re-etching. In addition, one surface of some of the specimens was electropolished [8] to permit metallographic examination. After this preparation, the specimens had a square cross-section ($\sim 3.6 \times 3.6$ mm^2) and a length between the shoulders of about 30 mm.

The chemical composition of these specimens was determined by X-ray fluorescence techniques, the average germanium concentrations being 23.3 at. % with a variation of $\pm$ 1.4 at. % over the length, this concentration being 1.4 at. % lower than that used in a previous study [5].

The mechanical properties were investigated with a Zwick 1386/0 deformation machine over a temperature range 20 to 615°C. At room temperature, the strain was determined directly whilst at higher temperatures, the strain was calculated from the crosshead displacement, due consideration being given to the hardness of the machine.

The specimens deformed at high temperatures were enclosed in a stainless steel tube containing forming gas and were heated by means of a three-zone vertical furnace, the temperature variation along the specimen being less than $\pm$ 1°C.

The temperature and strain-rate dependence of the mechanical properties in tension were investigated as were the mechanical properties in compression at 400°C in order that a comparison could be made with previous work [5].

After deformation, the side faces and the fracture surfaces of the deformed specimens were examined by both light and scanning electron microscopy, care being taken by repolishing to establish that the features observed were not restricted merely to the surface.

3. Results

3.1. Microstructure of the undeformed specimens

A photomicrograph and schematic representation of the germanium precipitates observed is shown in Figs. 3 and 2 respectively, whilst typical dimensions of the structure are shown in Table I.

TABLE I

	This work	W. R. Krummheuer, H. Alexander [5]
l	280 μm	330 μm
t	36 μm	28 μm
λ	87 μm	77 μm
d	3 μm	3 μm

This form of precipitation is similar to that reported to occur in the Al-Ge [3], Al-Si [2], and Ag-Si [2] systems.

3.2. Deformation

3.2.1. Modulus

The room temperature deformation curve of the eutectic, in which the strain was measured directly, consisted of two linear portions (stage I and stage II) which may be explained in terms of Kelly's theory for the deformation of fibre

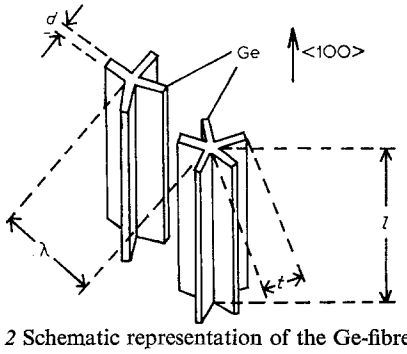

Figure 2 Schematic representation of the Ge-fibres.

Figure 3 Structure of the composite perpendicular to the axis (polished).

reinforced materials [9, 10]. Stage I corresponds to the elastic deformation of both components whilst stage II corresponds to the elastic deformation of the fibres and the plastic deformation of the matrix. The work-hardening curves obtained after repeated unloading and re-testing contained a successively larger stage I in each case due to the work-hardening which occurred during stage II of the previous deformation.

Metallographic examination of the specimens revealed that cracking of the germanium fibres contributed to the deviation from linearity observed towards the end of stage II.

The room temperature moduli for stage I and II were determined as 7.27×10^3 and 2.02×10^3 kg mm^{-2} respectively, the error being as large as $\pm$ 15% due to the small strains involved.

3.2.2. Work-hardening curves

The work-hardening curves, obtained as a function of temperature, are shown in Fig. 4 where it can be observed that with increasing temperature the alloy became increasingly ductile. As a result of slip line investigations, the initial linear portion of these curves was shown to correspond to stage II (stage I not being detectable without the use of direct strain measurements). At sufficiently high temperatures ($\geqslant$ 400° C), the initial linear portion was followed by a second with a smaller slope. This may be interpreted as part of stage III in which both components were ductile. At temperatures around 400° C a small region with zero slope was observed which in some cases resembled a type of yield phenomenon. In addition, a great variation of fracture strain with temperature was observed, the maximum fracture strain occurring at around 550° C (Fig. 5).

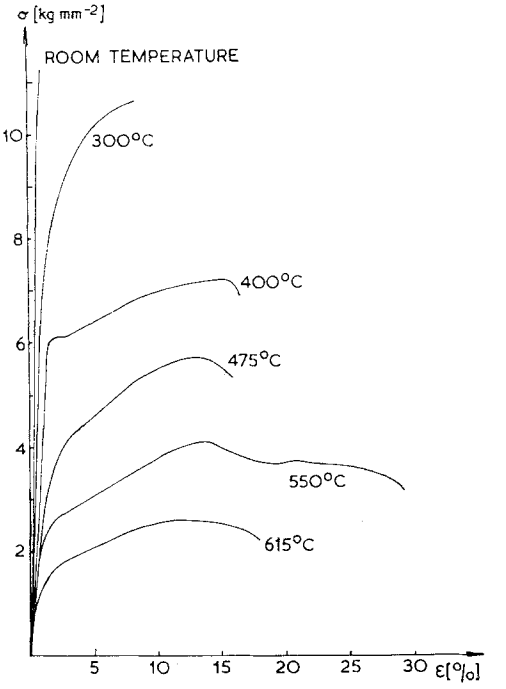

Figure 4 Stress-strain curves at different temperatures (tension).

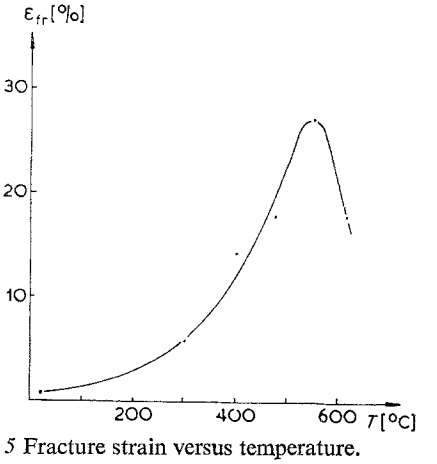

Figure 5 Fracture strain versus temperature.

A comparison of the work-hardening curves obtained during deformation in compression and tension at 300 and 475° C is shown in Fig. 6. A large difference in the work-hardening rates in the linear part of the stage III was observed, this difference being shown as function of temperature in Fig. 7. In addition, the corresponding values previously reported [5] for the matrix material are shown, these values being determined at 5% strain since the matrix compression curves had no linear portion.

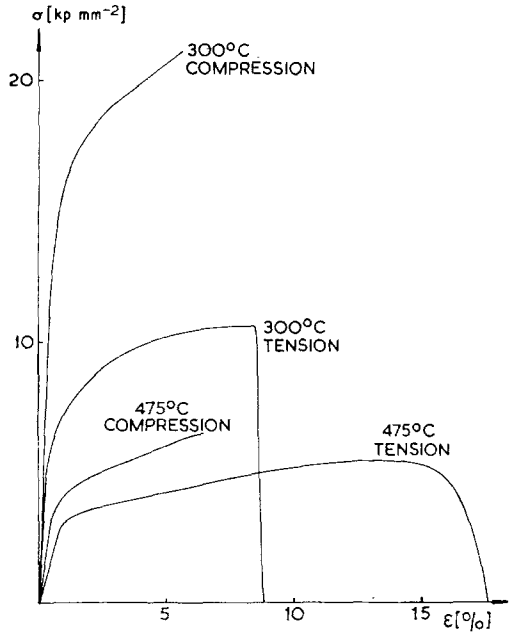

Figure 6 Comparison of compression and tension stress-strain curves.

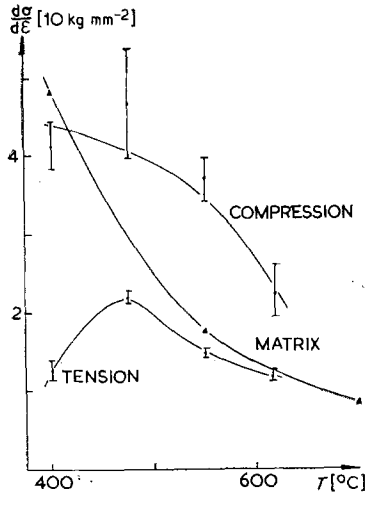

Figure 7 Work-hardening in the linear part of stage III for compression and tension tests and for the matrix at 5% strain.

At temperatures lower than 400°C, no true stage III existed. Differences between stage II in tension and compression were observed here too.

The ultimate tensile strength of the composite material, σ_{cu}, is shown as a function of temperature in Fig. 8 where it can be seen that at

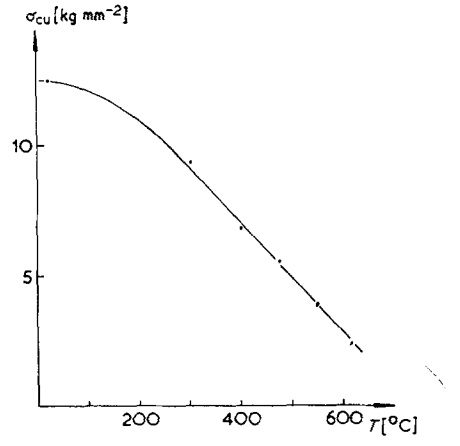

Figure 8 Ultimate tensile strength versus temperature.

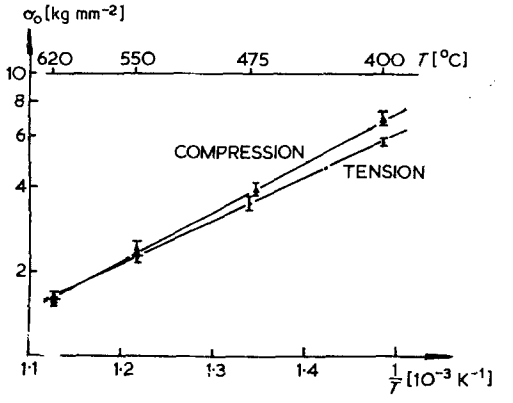

Figure 9 Transition stress, σ_0, from stage II to stage III versus temperature.

sufficiently high temperatures (> 300°C) a linear relationship was observed. A transition stress, σ_0, which can be defined as the extrapolated intersection of stages II and III was calculated and is shown in Fig. 9 together with similar values obtained from previous compression tests [5]. The following relationship was found to hold

$$\sigma_0 \sim \exp(Q/KT)$$

where

$Q = (0.31 \pm 0.02)$ eV in tension
$Q = (0.35 \pm 0.05)$ eV in compression.

For the dependence on strain-rate of the transition stress at 400 and 550°C, a relationship of the following form was determined

$$\sigma_0 = c \ln(\dot{\epsilon}/\dot{\epsilon}_0),\ \dot{\epsilon}_0 = 1\ \text{sec}^{-1}$$

where

$c = (0.8 \pm 0.11)$ kg mm^{-2} at 400°C
$c = (0.4 \pm 0.12)$ kg mm^{-2} at 550°C.

3.3. Metallography of the deformed specimens

3.3.1. Light microscopy

An examination of the specimens deformed at 20 and 300°C revealed broken germanium fibres with an average fragment length of 10 μm (Fig. 10) and 55 μm, respectively. The frequency of fibre fracture decreased with increasing temperatures and at 615°C no broken fibres were observed. An examination of photomicrographs like that in Fig. 10 also revealed a regular array of fracture sites with the fracture continuing into neighbouring fibres and a cone-shaped deformed area in the matrix adjacent to these sites.

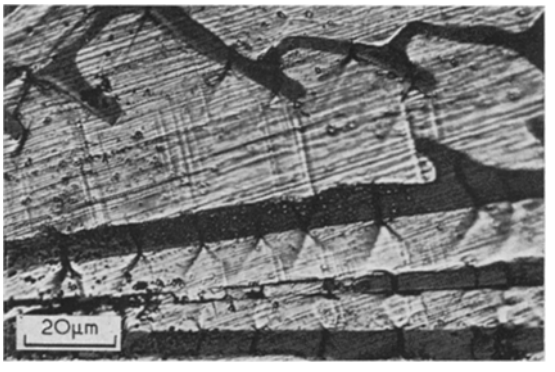

Figure 10 Surface of a specimen deformed at room temperature. Broken fibres and cone shaped deformed areas can be seen.

In the specimens deformed at 300°C, weak glide traces were observed in the germanium fibres whilst at higher temperatures, slip bands were readily observed. In the specimens deformed at 400°C many twins were observed in the matrix.

The macroscopic appearance of the fracture surface changed with temperature, at room temperature the fracture surface was smooth and perpendicular to the axis of the specimen with no observable notching. At higher temperatures ($\geqslant$ 400°C) however, notching became increasingly noticeable and the surface more split.

3.3.2. Scanning electron microscopy

The fracture surface of the specimen deformed at room temperature is shown in Fig. 11. The torn germanium fibres can be observed between the matrix ridges with the fracture continuing into the germanium fibre parallel to its axis. Specimens deformed at 300 and 400°C showed similar behaviour.

Side views of the fracture surfaces produced by deformation at 550 and 615°C are shown in Figs. 12 and 13, respectively. In Fig. 12, a germanium fibre only partly in contact with the matrix may be observed, whilst in Fig. 13, the fibres completely protrude from the matrix.

Photomicrographs of the side faces of the specimens about 5 mm from the fracture surface are shown in Figs. 14 to 18. The striking feature of Fig. 14 is the hole near the end of the fibre produced during deformation at 400°C. The same may be observed after deformation at 615°C (Fig. 18) but, in addition, the interface between the matrix and the fibre has opened. Similar features may be observed in Fig. 17, with the beginnings of matrix fracture, whilst in Fig. 16, after deformation at 550°C, broken matrix material may be observed. After deformation at 475°C, cracks in both fibres and matrix were observed (Fig. 15).

4. Discussion

4.1. Moduli

The modulus of a fibre reinforced material in stage I and II may be described by the following equations [9, 10].

$$E_{\mathrm{I}} = E_{\mathrm{f}}V_{\mathrm{f}} + E_{\mathrm{m}}V_{\mathrm{m}} \qquad (1)$$

$$E_{\mathrm{II}} = E_{\mathrm{f}}V_{\mathrm{f}} + (\mathrm{d}\sigma_{\mathrm{m}}/\mathrm{d}\epsilon)V_{\mathrm{m}}\,. \qquad (2)$$

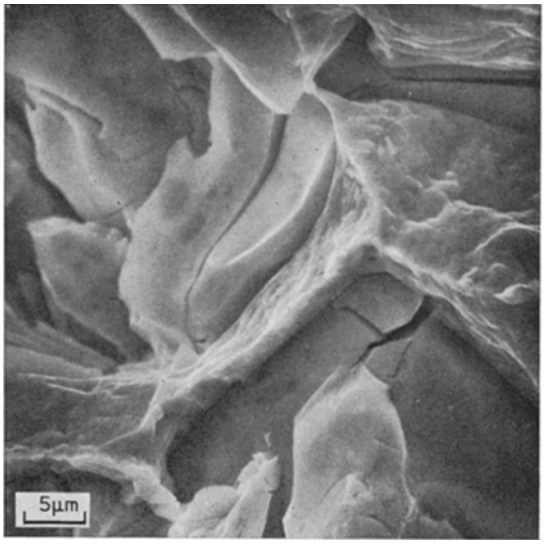

Figure 11 View onto a fracture surface produced at room temperature.

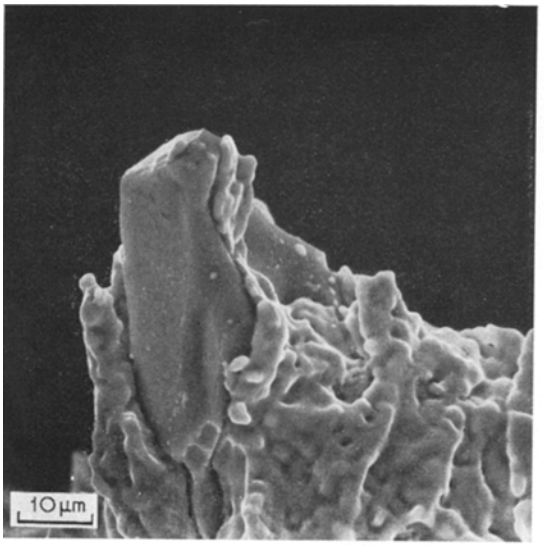

Figure 12 Side-view of a fracture surface produced at 550°C. Note the free surface of Ge-platelet.

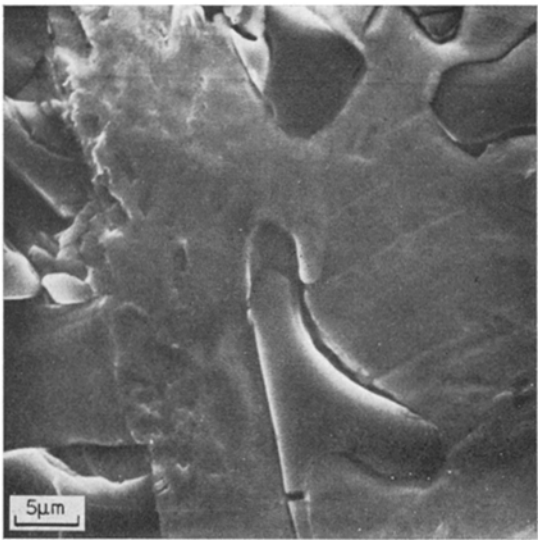

Figure 14 Side-view: hole in the matrix at the end of a Ge-fibre. Deformation temperature, 400°C.

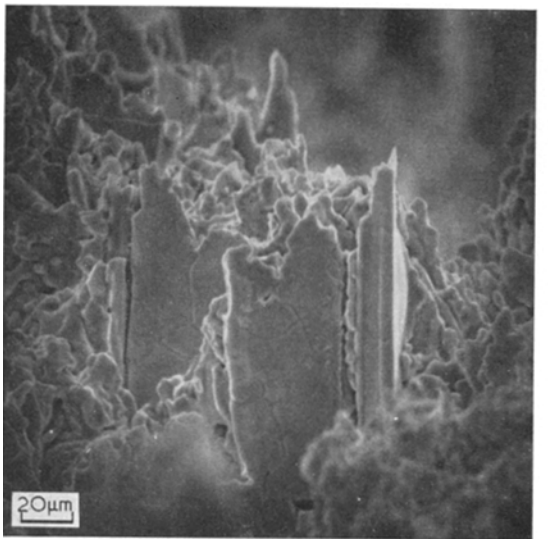

Figure 13 Same as Fig. 12 but 615°C. Protruding Ge-fibres.

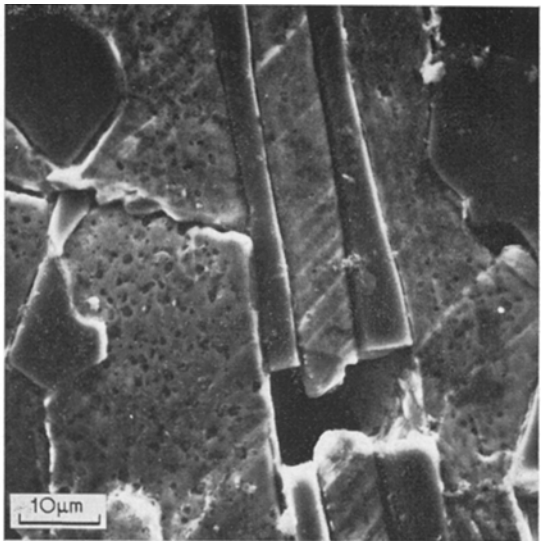

Figure 15 Side-view: cracks in fibres and matrix. Deformation temperature, 475°C.

Generally, the term $(d\sigma_m/d\epsilon)V_m$ may be neglected (except when the fibre diameters and distances are small [11-13] $\sim$ 5 µm). It has been shown [14] that for larger distances, the dislocation arrangement is such that the term $(d\sigma_m/d\epsilon)V_m$ cannot be greater than in the pure matrix material and, hence, it is permissible in this work because of the dimensions of the microstructure used to make the assumption $(d\sigma_m/d\epsilon)V_m \ll E_f V_f$. As $E_f = E_{\langle 100 \rangle} = 10.4 \times 10^3$ kg mm^{-2} [15], V_f may be calculated from Equation 2 as (19.2 $\pm$ 2.9) %. Hence, substituting this value into Equation 1 yields a value for E_m of (6.5 $\pm$ 2.1) 10^3 kg mm^{-2}.

The fibre volume thus calculated is about 20% lower than that calculated from the phase diagram based on the assumption of restricted germanium diffusion in the matrix at lower temperatures. This difference can be attributed to that portion of germanium which forms fibres

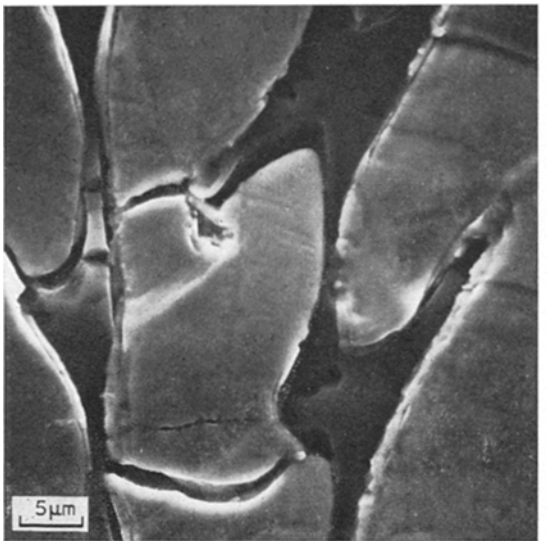

Figure 16 Side-view: broken matrix material. Deformation temperature, 550°C.

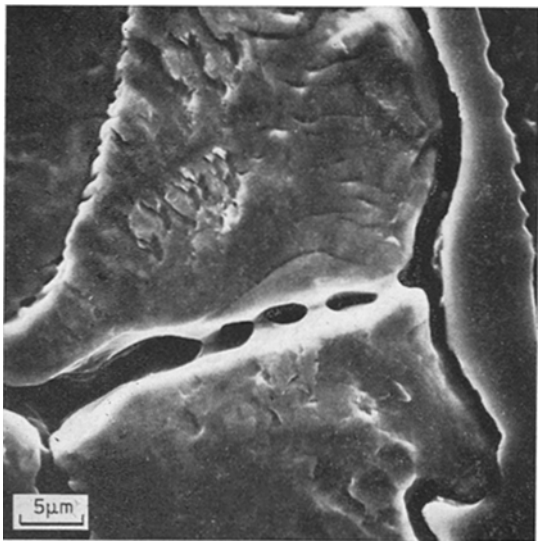

Figure 17 Side-view: opened interface, beginning matrix failure. Deformation temperature, 615°C.

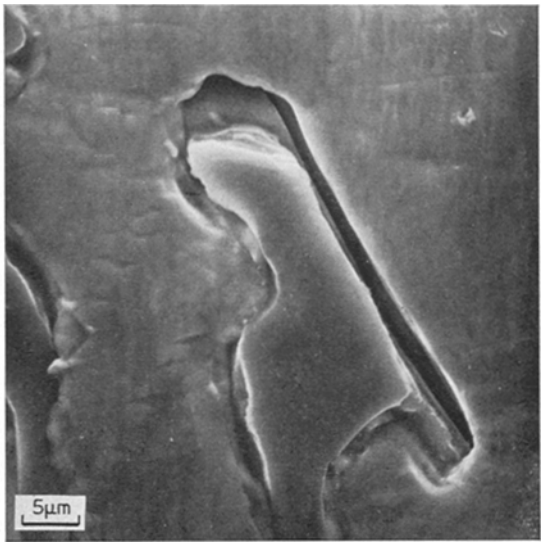

Figure 18 Side-view: hole near the end of a Ge-fibre, opened interfaces. Deformation temperature, 615°C.

smaller than the critical length. The error in $E_m(\pm 30\%)$ is due to the uncertainty in the measurement of E_I and E_{II}. Within this range, however, the result agrees with the values reported for a Ag-4 at.% Ge solid solution ($E = 8.1 \times 10^3$ kg mm^{-2}) [16].

4.2. The difference between compression and tension at lower temperatures

A similar difference to that observed in this work between the stress in compression and tension during stage II has been reported for a (Co, Cr) – $(CrCo)_7C_3$ eutectic [17, 18]. This was attributed to the differences in the coefficient of thermal expansion and, hence, a similar explanation will be attempted here.

During cooling of the eutectic stresses may arise if the coefficients of thermal expansion (α_m, α_f) are different. Above a certain temperature, T_0 (the stress relaxation temperature), these stresses are relaxed by creep, whilst below T_0 they are frozen in. If $\alpha_m > \alpha_f$ these residual stresses are tensile in the matrix and compressive in the fibres. The transition from stage I to stage II will, therefore, occur in a tensile test at lower stress than in a compressive test. The difference in these transition stresses is given by [18]

$$\triangle\sigma = 2V_f E_f \triangle \alpha \triangle T$$

where

$$\triangle \alpha = \alpha_m - \alpha_f \text{ and } \triangle T = T_0 - T .$$

It has been suggested [18] that this theory could explain a similar difference in stage II, provided the matrix and fibre strains were small and identical. Assuming that these arguments are valid to the end of stage II, a distinction must be made between brittle and ductile fibres [19].

If the fibres are ductile, the end of stage II must occur at higher stresses in a tensile test compared with a compressive test, because of the compressive stresses in the fibres. If the fibres are brittle, however, the end of stage II is due to the

fibres fracturing, such fibre fracture occurring at higher stresses in compression than in tension. In a composite material, therefore, with brittle fibres the material could be loaded in compression to higher stresses than in tension, regardless of the residual stresses. It seems that such behaviour was observed in this work. This is supported by the disappearance of this difference at temperatures higher than 475°C so it may be concluded that the stress relaxation temperature T_0 is slightly less than 475°C.

4.3. Dependence of σ_0 on temperature and strain-rate at high temperatures

The temperature dependence of σ_0 may be described by

$$\sigma_0 \sim \exp(Q/KT); \quad Q = (0.31 \pm 0.02)\,\text{eV}.$$

The energy Q agrees well with that found in a previous compression study [5]. There are, however, differences in the strain-rate dependence. In compression

$$\sigma_0 \sim (\dot{\epsilon}/\dot{\epsilon}_0)^n; \quad n = 0.19, \quad \dot{\epsilon}_0 = 1\ \text{sec}^{-1}$$

where n is independent of temperature. In tension, however, it must be assumed that n is temperature dependent with

$$n = (0.14 \pm 0.02) \text{ at } 400°\text{C}$$
$$n = (0.19 \pm 0.02) \text{ at } 550°\text{C}.$$

An attempt to explain these relationships solely by considering the mechanical properties of germanium failed since the lower yield stress has been shown to be of the form [7]

$$\sigma_{LY} \sim \dot{\epsilon}^{1/(m+2)} \exp[E/(m+2)KT]$$
$$E = (1.62 \pm 0.06)\,\text{eV}$$
$$m = 1.1.$$

A TEM investigation [20] of the specimens deformed in compression, however, indicated that for deformation temperatures in excess of 400°C interface sliding had also to be taken into consideration. This was shown by determining the dislocation density in the fibre and the matrix and, hence, estimating the average strain. The results of these calculations indicated that the average fibre strain and the strain in the composite differed considerably, a result which was also confirmed by scanning electron microscopy (Figs. 14 and 18). It was concluded, therefore, that the dependence of σ_0 on temperature and strain-rate were governed more by the properties of the interface than by the mechanical properties of the germanium.

4.4. Yield point

A similar yield phenomena to that observed in this work has also been reported to occur in Cu – Fe [21] and Cu – Mo [22] composite. This behaviour may, in the present work, be attributed to the yield point of germanium whilst in the other systems mentioned to that of Fe and Mo, respectively.

A criterion for the observation of the yield point may be derived by considering the rule of mixture and interface sliding ($\epsilon_f \neq \epsilon_m$) and by assuming equal strains in the matrix and in the composite as a whole, i.e.

$$(\epsilon_c = \epsilon_m = \epsilon)$$

hence

$$d\sigma_c/d\epsilon = V_m(d\sigma_m/d\epsilon) + V_f(d\sigma_f/d\epsilon_f)(d\epsilon_f/d\epsilon). \quad (3)$$

In the region between the upper and lower yield point, $d\sigma_f/d\epsilon_f < 0$ so the condition for the observation of the yield point may be determined as

$$|V_f(d\sigma_f/d\epsilon_f)(d\epsilon_f/d\epsilon)| \geqslant V_m(d\sigma_m/d\epsilon).$$

The disappearance of yielding may be attributed to the yield point associated with germanium becoming less pronounced with increasing temperature [7].

4.5. Work-hardening

The difference in the rate of work-hardening in the linear part of stage III during compression and tension for sufficiently high temperatures ($T \geqslant 400°\text{C}$) is one of the most striking results of this work. As all the terms on the right hand side of Equation 3 are known, $d\sigma_c/d\epsilon$ may be calculated ($d\sigma_f/d\epsilon_f$ is taken from the work of Patel *et al* [23], $d\sigma_m/d\epsilon$ from Krummheuer *et al* [5], and $d\epsilon_f/d\epsilon$ may be extrapolated from Bojowald's work [20]). Thus, at 400°C a value of 43 kg mm^{-2} is calculated for $d\sigma_c/d\epsilon$ which is in fair agreement with the values measured in compression (Fig. 7). At all other temperatures, the calculated values, for some reason which is not clearly understood at present, are smaller than those determined experimentally.

In tension, $d\epsilon_f/d\epsilon$ is not yet known over the whole range of temperature so an attempt was made to calculate from Equation 3 $V_f(d\sigma_f/d\epsilon_f)(d\epsilon_f/d\epsilon)$ as a function of temperature from the measured $d\sigma_c/d\epsilon$ and the known $V_m(d\sigma_m/d\epsilon)$ [5]. This parameter is plotted in Fig. 19 where it can be seen that, for temperatures up to 475°C, a negative value is obtained. This can be explained by assuming that the germanium is still in the yielding region during this stage of deformation. This assumption is supported by

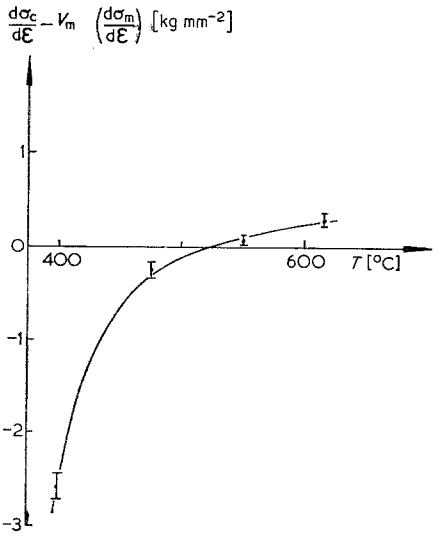

Figure 19 $V_f(d\sigma_f/d\epsilon_f)$ $(d\epsilon_f/d\epsilon)$ versus temperature.

the observation of a hole near the end of a fibre deformed at 400°C (Fig. 18), which implies that $\epsilon_f < \epsilon$, and by a TEM investigation of specimens deformed in tension at 400°C to $\epsilon = 6\%$. From the dislocation density measured in the fibres, an average fibre strain of 1.8% was calculated [24] which lies in the yield region of ⟨100⟩ – Ge [23].

It would appear, therefore, that interface sliding operates more strongly and at lower temperatures in tension than in compression; however, for a full explanation of this part of the work a detailed TEM study is at present in progress.

4.6. Fracture

During high temperature fracture, it is the matrix that fails first while during low temperature fracture it is the fibres. If the matrix fails, the fracture of the composite is governed by interfacial sliding, composite fracture not occurring if

$$\tau U l \geqslant \sigma_{mu} F_m$$

where τ is the shear stress at the interface, U is the circumference of the fibre, l the distance from the fracture site to the end of the fibre, σ_{mu} the ultimate tensile strength of the matrix, and F_m the area of the matrix between two fibres. With the relation $U = F_f/\alpha$ (where the geometrical factor α can be estimated as $\sim$ 1.5 μm from Table I)

$$l \geqslant (\sigma_{mu}/\tau)\, \alpha\, (V_m/V_f)\,. \qquad (4)$$

From this inequality the plot of fracture strain versus temperature (Fig. 5) can be understood qualitatively. At 550°C, the composite could be strained a further 10%, after the onset of matrix fracture, before failure of the composite occurred. The fracture surface is shown in Fig. 12 where it can be seen that one germanium fibre serves as a sliding path. At 615°C, however, the interface could not retard the fracture (because Relation 4 was not satisfied on account of the small τ at this temperature) and, hence, the fibres protrude from the fracture surface (Fig. 13).

Since Relation 4 is not valid at 615°C the shear stress at the interface may be estimated by setting l equal to half of the average fibre length and taking σ_{mu} from the compression deformation curves [5] to yield $\tau < 0.12$ kg mm^{-2} at 615°C. Fracture toughness of this kind caused by delamination of the interface has been reported in the Cu-W [25] and Cu-Fe [26] systems.

At low temperatures ($\leqslant$ 300°C) fracture is initiated by fibre failure. This failure begins at the first deviation from the linear stress-strain relationship and is not connected with sudden fracture of the specimen. According to Kelly [9], this is possible if the matrix can resist the load takeover by work-hardening. The mathematical condition may be shown to be

$$(\sigma_{mu} - \sigma_{m'})/\sigma_{fu} \geqslant (V_f/V_m)$$

where $\sigma_{m'}$ is the stress in the matrix at the moment of fibre fracture and σ_{fu} is the ultimate tensile strength of the fibres.

All the features noted during metallographic examination, such as the regular arrangement of the sites of fibre fracture, the cone shaped deformed regions in the matrix and the ridges of matrix between fibres, point to a high shear strength of the interface the value of which may be estimated from the ultimate tensile strength of the composite, σ_{cu}. σ_{cu} is given by the ultimate tensile stress of the matrix, σ_{mu}, plus the load transferred to the broken fibres by the interface shear stresses [10, 27] i.e.

$$\sigma_{cu} = \sigma_{mu}(1 - V_f) + (\tau l'/4\,\alpha)V_f$$

where l' is the average length of broken fibres. Hence, at room temperature, $\tau \sim$ 14 kg mm^{-2} which is twice as large as that obtained for Al_2O_3-Ni composites [28].

The temperature dependence of τ appears to be much stronger than that observed in Cu-Mo composites [22] in which no failure by interface sliding occurred. In the temperature range 400 to 475°C the fracture mode changes as can

be seen in Fig. 19 where cracks can be observed in both the fibres and the matrix.

5. Summary

The unidirectionally solidified Ag-Ge eutectic has been investigated by dynamic tensile deformation and by light and scanning electron microscopy and comparisons have been made with previous compression tests [5]. Two temperature dependent processes had to be considered to explain the results, that of increasing germanium ductility and that of decreasing interface shear strength with increasing temperature.

The range of temperature over which the various effects were observed are shown in Table II.

TABLE II

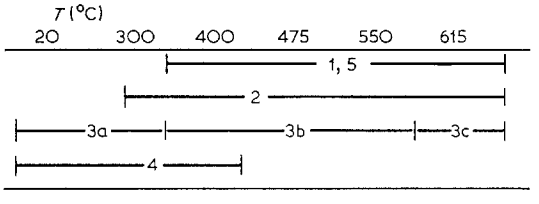

1. Interface sliding. The maximum fracture strain at 550° C could be explained by this effect. It seems that interface sliding operated more strongly in tension.

2. Plastic deformation of both components.

3. Interface shear strength more dependent on temperature than the ultimate tensile strength of the matrix. This caused different fracture behaviour over the range of temperature: (a) deformation curves showed a stage caused by statistical fracture of the fibres (high shear strength); (b) transition region; (c) fracture initiated by matrix failure (low shear strength).

4. Compression specimens could be loaded to higher stresses due to higher brittle fracture stress in compression.

5. Work-hardening in stage III lower in tension than in compression.

Acknowledgements

The authors wish to thank Dr E. A. Thompson for a discussion of the thermal induced residual stresses, Dr Horstmann for advice concerning the scanning electron microscopy results and Dr S. Trojanova for the communication of the unpublished results of Professor Dr U. Koester. We are indebted to Mr R. Booth for redrafting the manuscript.

The scanning electron microscopy was performed at the "Institut für Werkstofforschung" of the "Deutsche Forschungs- und Versuchsanstalt für Luft- und Raumfahrt (DFVLR)". For the help in taking the photomicrographs we are indebted to Dr Dudeck and Mr Borath.

The alloy was prepared at the "Institut für Metallphysik der Universität Göttingen" and for these facilities thanks are due to Professor Dr P. Haasen.

The testing machine and other equipment was kindly supplied by the "Volkswagenstiftung".

References

1. A. HELLAWELL, *Progr. Mat. Sci.* **15** (1970) 3.
2. M. G. DAY and A. HELLAWELL, *Proc. Roy. Soc. Lond.* **A305** (1968) 473.
3. A. HELLAWELL, *Trans. Met. Soc. AIME* **293** (1967) 1049.
4. I. MIURA and H. HAMANAKA, *J. Jap. Inst. Metals* **32** (1968) 898.
5. W. R. KRUMMHEUER and H. ALEXANDER, *Z. Metallk* **62** (1971) 129.
6. M. HANSEN and K. ANDERKO, "Constitution of Binary Alloys", 2nd Edn. (McGraw-Hill, New York Toronto, London, 1958).
7. H. ALEXANDER and P. HAASEN, *Solid State Phys.* **22** (1968) 28.
8. G. REINACHER, *Z. Metallk.* **48** (1957) 162.
9. A. KELLY and G. J. DAVIS, *Met. Rev.* **10** (1965) 1.
10. A. KELLY, "Strong Solids" (Clarendon Press, Oxford, 1966).
11. A. KELLY and W. LILHOLT, *Phil. Mag.* **19** (1969) 311.
12. R. KOSSOWSKY, W. L. JOHNSTON and B. J. SHAW, *Trans. Met. Soc. AIME* **245** (1969) 1219.
13. P. NEUMANN and P. HAASEN, *Phil. Mag.* **20** (1970) 285.
14. M. R. PINNEL and A. LAWLEY, *Met. Trans.* **1** (1970) 1337.
15. H. B. HUNTINGTON, *Solid State Phys.* **7** (1958) 213.
16. S. TROJANOVA, private communication.
17. E. R. THOMPSON, D. A. KOSS and D. C. CHESNUTT, *Met. Trans.* **1** (1970) 2807.
18. D. A. KOSS and S. M. KOPLEY, *ibid* **2** (1971) 1557.
19. E. A. THOMPSON, private communication.
20. J. BOJOWALD, Diploma thesis, Köln 1972.
21. G. GARMONG and L. A. SHEPHARD, *Met. Trans.* **2** (1971) 175.
22. A. KELLY and W. R. TYSON, *J. Mech. Phys. Solids* **13** (1965) 329.
23. J. R. PATEL and A. R. CHAUDHURI, *J. Appl. Phys.* **34** (1963) 788.
24. J. ALBRECHT, private communication.
25. G. A. COOPER and A. KELLY, *J. Mech. Phys. Solids* **15** (1967) 279.

26. S. FLOREEN, H. W. HAYDEN and R. M. PILLIAR, *Trans. Met. Soc. AIME* **245** (1969) 2529.
27. J. P. CAHOON and H. W. PAXTON, *ibid* **245** (1969) 1401.
28. C. A. CALOW and A. MOORE, *J. Mater. Sci.* **7** (1972) 543.

Received 12 April and accepted 26 August 1973.